Variation of Bremsstrahlung Intensity With Angle Near the High-Energy End of the Spectrum*

R. ZDARKO, D. DRICKEY, AND R. MOZLEY
High-Energy Physics Laboratory, Stanford University, Stanford, California
(Received 14 August 1964)

We have measured the relative intensity of thin-target bremsstrahlung as a function of bremsstrahlung angle at the high-energy end of the spectrum in the angular range from 0.0 to 3.0 mc^2/E for peak energies of $E=375$ and 550 MeV. Our measurements are compared with the theories of Schiff and of Olsen and Maximon; there is substantial disagreement.

INTRODUCTION

THE effects of the approximations used in calculating the bremsstrahlung spectrum are most prominent for photon energies near the maximum energy allowed by energy conservation. Here, the second Born approximation, final-state interactions, and the various screening approximations can produce a significant variation in the calculated bremsstrahlung shape. Most of these approximations also produce differences in the calculated angular distribution, i.e., the variation of bremsstrahlung intensity with angle. We have measured the relative bremsstrahlung angular distribution near the high-energy end of a 375-MeV spectrum and at a point between the high- and low-energy ends of a 550-MeV spectrum in order to test some of these approximations.

By observing the π^0 photoproduction reaction, one can select an energy interval from the incident photon beam and measure the intensity of this reaction relative to an ion chamber monitoring the photon beam. Since the photoproduction reaction will be proportional to the number of photons in this energy interval, measurements of the ratio of π^0 counts to ion chamber reading will then produce relative measurements of the bremsstrahlung angular distribution.

EXPERIMENTAL METHODS

The experimental arrangement is similar to that used in previous polarized photon experiments.[1-3] The undeflected electron beam from the Stanford Mark III linear accelerator struck a thin ($\approx$0.001 radiation length) aluminum radiator. After passing through the radiator, the electrons were deflected, their energy measured to $\approx\pm1\%$, and their energy spectrum monitored and maintained at $\approx\pm1\%$. The photon beam was collimated with a $\frac{3}{8}$-in.-diam collimator 425 in. from the radiator and passed through a liquid-hydrogen target. The photon intensity was monitored with an ion chamber. Photon intensity in a selected energy interval was measured by observing the momentum-analyzed recoil proton from π^0 photoproduction in the hydrogen target.

Data were taken at photon angles α between 0.0 and 3.0 (measured in units mc^2/E, where m is the electron mass and E the electron beam energy) and at photon energies $\epsilon=0.86$ and 0.58 (ϵ is the reduced energy, i.e., the ratio of the photon and incident electron energies).

Bremsstrahlung angles were selected by means of Hemholtz coils located sufficiently near the radiator so that electron beam angle changes did not appreciably change the electron beam position on the radiator. The coil currents corresponding to a given angular deflection were determined by observing the distance of deflection of the electron beam at a point 402 in. from the coils when the sweeping magnet was turned off. We estimate an angular error of ±0.05 mc^2/E in measuring and setting the bremsstrahlung angle. The effects of this error should be negligible and have not been included in our data. The angle 0.0 mc^2/E was determined for each run by sweeping with a separate set of coils to the angle of maximum intensity as observed with the ion chamber. "Centering" was performed in both the vertical and horizontal planes. We estimate 0.0 mc^2/E to be determined to an accuracy of 0.1 mc^2/E.

In order to minimize uncertainties in centering and to cancel effects due to polarization of the bremsstrahlung, data at a given angle were taken by deflecting the beam in quadrature about the central position. Explicitly, data at each angle were the sum of data taken with the beam deflected right, down, left and up, each deflection being triggered by a constant amount of integrated current measured with the photon beam monitor. Cycling several times minimized short-term effects due to transient beam angular fluctuations and inaccuracies in measuring the integrated voltage for each cycle. Beam position on the radiator and "centering" to 0.0 mc^2/E were periodically checked for drift, and small corrections were made when necessary. Protons were counted with two counter telescopes located in the magnet focal plane, each telescope being made of two plastic scintillation counters. Pulse-height analysis and a coincidence between the two scintillators provided adequate proton identification.

The central energy of the photon producing the observed protons was determined by a yield curve, i.e., the experimental determination of counting rate as the

* This work was supported in part by the U. S. Navy Office of Naval Research and the U. S. Air Force, Office of Scientific Research.
[1] R. E. Taylor and R. F. Mozley, Phys. Rev. 117, 835 (1960).
[2] R. C. Smith and R. F. Mozley, Phys. Rev. 130, 2429 (1963).
[3] D. J. Drickey and R. F. Mozley, Phys. Rev. 136, B543 (1964).

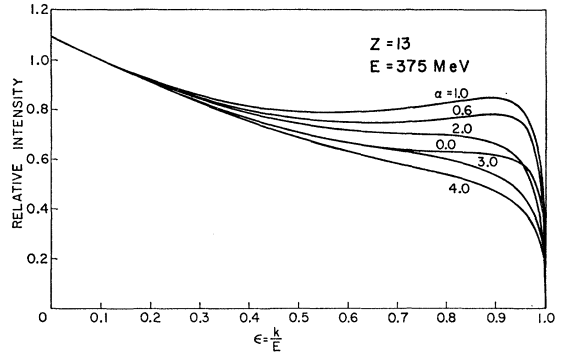

FIG. 1. Relative bremsstrahlung intensity versus reduced photon energy from a thin aluminum radiator using the theory of Olsen and Maximon. Each curve represents the intensity at a reduced angle α normalized at $\epsilon=0.1$ ($\alpha=E\theta/mc^2$, where θ=photon angle in radians).

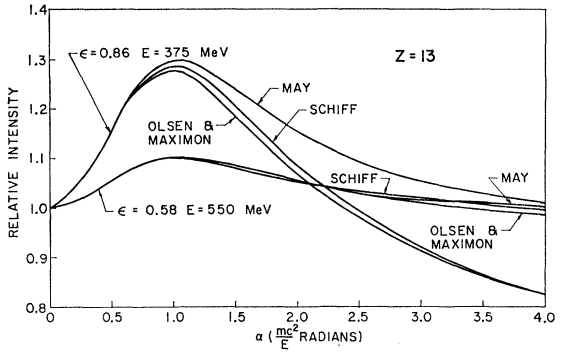

FIG. 2. Relative bremsstrahlung intensity versus reduced angle for two values of ϵ, assuming a thin-walled ion chamber with a low-energy cutoff of 30 MeV as the normalization monitor.

electron beam energy was lowered in steps to an energy below threshold for the particular spectrometer setting.[3] The fold of the bremsstrahlung shape with the magnet photon resolution function then determined the photon energy being observed.

MULTIPLE SCATTERING AND FINITE COLLIMATOR EFFECTS

The theoretical curves for a radiator sufficiently thin to neglect multiple scattering of the electrons show a rise in relative intensity at an angle $\alpha\approx 1\ mc^2/E$ (see Fig. 1). In our thin 0.001 radiation length foil, the electrons multiple scatter through a mean angle of the same order. We have calculated this effect as in previous experiments[1–4] by measuring the spatial intensity distribution of scattered electrons in a plane near the collimator with glass slides and folding this distribution into the bremsstrahlung angular distribution expected from a beam which does not multiple scatter. This experimental method also compensates for finite beam size and beam angular divergence effects. Additionally, the collimator used in this experiment subtends an angle of 0.68 mc^2/E at 375 meV and 1.0 mc^2/E at 550 MeV. The finite collimator size was folded into the results of the multiple scattering fold to obtain our final theoretical curves of the expected bremsstrahlung angular distribution.

BACKGROUNDS

Empty target counting rates in this experiment were found to be negligible. At this photon energy (335 MeV), the proton Compton effect is also negligible. The only background found to be significant was observed by running with the radiator removed. Since this work was performed in the "straight through beam" area of the Stanford accelerator, photons produced inside the machine can produce a bremsstrahlung intensity comparable to that produced from the radiator, especially at the larger bremsstrahlung angles. We have taken "radiator out" runs at each bremsstrahlung angle and subtracted the observed counts from the main counting rate and also subtracted the observed ion chamber current from that observed with the foil in. This background run was normalized by using a secondary emission monitor (SEM) to monitor the deflected electron beam current. The SEM used for this subtraction was placed directly after the sweeping magnet and has been shown to be reproducible to about 5%. We have included this error in our error analysis.

We have attempted to measure a possible photon monitoring error caused by collimator penetration and secondary gamma production. Such secondary effects should produce photons at larger angles than the collimated beam. The ratio of counting rates measured in the normal manner to that measured with a second collimator placed immediately in front of the ion chamber but not intersecting the main photon beam was 1.014 ± 0.01. We conclude that penetration and regeneration of soft photons are negligible for this experiment. First-order penetration effects were found to be negligible by simply plugging the collimator.

THEORY AND RESULTS

To show the relative angular distribution at a given value of ϵ, the theoretical curves for each angle must be

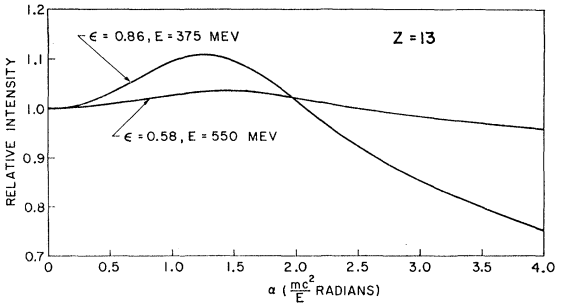

FIG. 3. The Schiff curves of Fig. 2 modified by the multiple scattering, finite collimator and beam size, and beam angular divergence.

[4] R. F. Mozley, R. C. Smith, and R. E. Taylor, Phys. Rev. 111, 647 (1958).

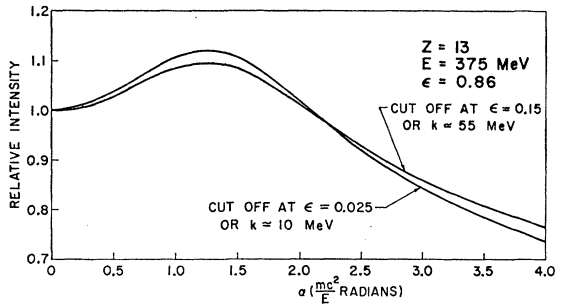

FIG. 4. The $\epsilon=0.86$ curve of Fig. 3 demonstrating the effect of the low-energy cutoff choice.

normalized. Customarily (as in Fig. 1) the curves are normalized near $\epsilon=0.0$. However, in our experiment the ion chamber monitoring the photon beam provided the basis for such a normalization. We have measured the ion chamber sensitivity as a function of peak bremsstrahlung energy between 200 and 500 MeV. Its sensitivity is consistent with a uniform sensitivity to photons of all energies larger than 30 MeV. This could be expected since the total attenuation cross section as a function of energy for photons is relatively flat above 30 MeV. Photons below 30 MeV are strongly attenuated by the ≈ 7 g/cm^2 of material in the beam path in front of the ion chamber. We have, therefore, normalized the calculated curves by assuming uniform sensitivity of the ion chamber to an $N(k)$ spectrum with a low-energy cutoff at 30 MeV.

Oy the other hand, a very thin-walled ion chamber with no attenuation might be expected to be sensitive only to the low-energy photons (normalization near $\epsilon=0$) while a thick-walled ion chamber is sensitive to the integral of $kN(k)$. These are clearly limiting cases and have been plotted as dashed curves in our figures.

The theories of Schiff[5,6] and Olsen and Maximon[6,7] were used for comparison. They are both extreme relativistic small-angle formulas. The Schiff theory uses Born approximation with an approximate exponential screening potential; the Olsen and Maximon theory is Coulomb corrected, includes an intermediate screening correction, and should be the more accurate. Within the sensitivity of our experiment, these theories are indistinguishable, and we have used them interchangeably for comparison with our results. We have also examined the theory of May[8] but his formulas are given in terms of a screening function defined only in the complete screening limit. Hence, a realistic comparison is not valid since, at angles larger than 1 mc^2/E, our experiment is sensitive to the screening function.

The calculated curves for these theories are given in Fig. 2. The relative change in intensity for $\epsilon=0.58$ and $\epsilon=0.86$ is shown, the curves being set equal to 1.0 at $\alpha=0.0$ for convenience of presentation. In this figure, the curves of Schiff and Olsen and Maximon differ by no more than 1.5%. The divergence of the May theory due to the use of the complete screening approximation is clearly seen.

Figure 3 shows these same curves for the Schiff theory but now modified to our experimental condition by the fold of multiple scattering, finite collimator and beam size, and beam angular divergence as described above.

Figure 4 shows the effect of using different low-energy cutoffs for the normalization of the $\epsilon=0.86$ curve. Curves are given using a cutoff at 10 MeV ($\epsilon\approx 0.025$) and at 55 MeV ($\epsilon\approx 0.15$). Since the shape of the curves changes only slightly (from 0 to 3% difference) for such a large change in cutoff energy, the actual cutoff used is not of major importance.

Figures 5 and 6 present our results at $\epsilon=0.58$ and 0.86, the data points being plotted as ratios to the point at $\alpha=0.0$. The solid curve is for a thin-walled ion chamber with a cutoff at 30 MeV as was our experimental situation. The dotted curves are the extreme

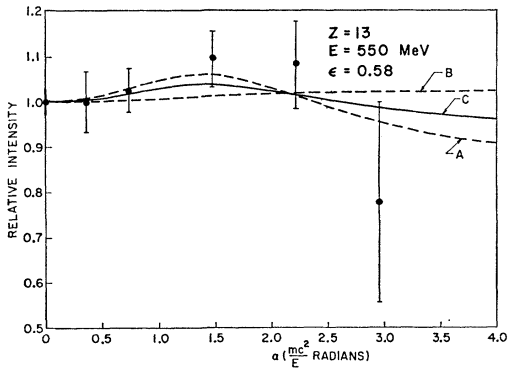

FIG. 5. Comparison of the experimental results at $\epsilon=0.58$ with the theory of Schiff. Curve B assumes a thick-walled monitor, curve A assumes a thin-walled monitor with no cutoff, while curve C assumes a thin-walled monitor with a 30-MeV cutoff.

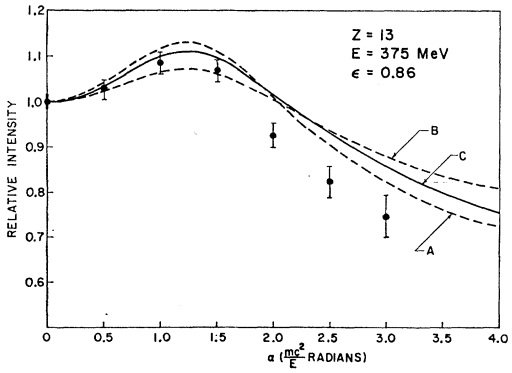

FIG. 6. Comparison of the experimental results at $\epsilon=0.86$ with the theory of Schiff. Curve B assumes a thick-walled monitor. Curve A assumes a thin-walled monitor with no cutoff, while curve C assumes a thin-walled monitor with a 30-MeV cutoff.

[5] L. Schiff, Phys. Rev. **83**, 252 (1951).
[6] H. W. Koch and J. W. Motz, Rev. Mod. Phys. **31**, 920 (1959).
[7] H. Olsen and L. C. Maximon, Phys. Rev. **114**, 887 (1959).
[8] M. May, Phys. Rev. 84, 265 (1951).

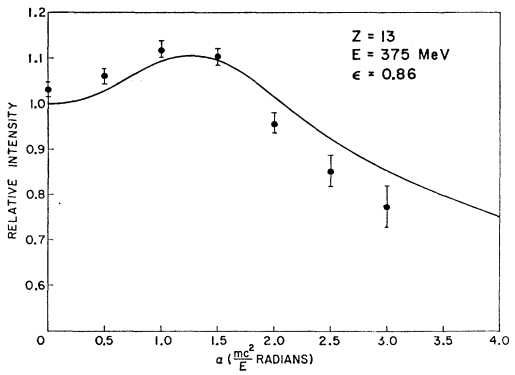

FIG. 7. χ^2 fit of the $\epsilon=0.86$ data to curve C of Fig. 6. The probability for this curve to fit our data is less than 0.01.

limiting cases assuming a thin-walled ion chamber with no cutoff (curve A) and assuming a thick-walled ion chamber or quantameter (curve B).

At $\epsilon=0.58$ the results are in substantial agreement with the theory, although the statistics are poor. In Fig. 6 the results for $\epsilon=0.86$ show a pronounced disagreement with the theoretical curve and its two limiting cases.

We have also made a one-parameter χ^2 fit of the data to the calculated curve of Fig. 6. Figure 7 shows the resultant data, the χ^2 test giving a probability less than 0.01 for agreement. Even when fitted to the lower limiting case (curve A) the χ^2 test gives a probability less than 0.02. We conclude that the observed relative intensity near the high-energy end of the bremsstrahlung spectrum decreases more rapidly with angle than predicted by the theories investigated.

ACKNOWLEDGMENTS

Dr. F. F. Liu and E. Maninger aided us materially with the experimental equipment and data taking. Dr. R. H. Pratt has contributed many helpful comments concerning the theory.

APPENDIX

The following formulas were used to calculate our theoretical curves. In all formulas we define ϵ, α, and C as

$$\epsilon=\frac{k}{E},\quad \alpha=\frac{E\theta}{mc^2},\quad \text{and}\quad C=\frac{8Z^2e^2}{\hbar c}\left(\frac{e^2}{mc^2}\right)^2.$$

(A). From Schiff [Eq. (1) of Ref. 5, and formula 2BS of Ref. 6],

$$d\sigma_{k,\theta}=C\frac{d\epsilon}{\epsilon}\frac{\alpha d\alpha}{(1+\alpha^2)^2}\left\{\frac{8\alpha^2(1-\epsilon)}{(1+\alpha^2)^2}-2\left(1-\epsilon+\frac{\epsilon^2}{4}\right)+\ln[M(\alpha,\epsilon)]\left[1-\epsilon+\frac{\epsilon^2}{2}-\frac{2\alpha^2(1-\epsilon)}{(1+\alpha^2)^2}\right]\right\},$$

where

$$\frac{1}{M(\alpha,\epsilon)}=\left(\frac{\epsilon mc^2}{2E(1-\epsilon)}\right)^2+\left(\frac{Z^{1/3}}{111(1+\alpha^2)}\right)^2;$$

(B) From May [the sum of Eqs. (5) and (6) in Ref. 8]:

$$d\sigma_{k,\theta}=C\frac{d\epsilon}{\epsilon}\frac{\alpha d\alpha}{(1+\alpha^2)^2}\left\{-2(1-\epsilon)\left(\frac{1-\alpha^2}{1+\alpha^2}\right)^2-\frac{\epsilon^2}{2}+\ln\left[\frac{(1+\alpha^2)^2}{f^2}\right]\left[1-\epsilon+\frac{\epsilon^2}{2}-\frac{2\alpha^2(1-\epsilon)}{(1+\alpha^2)^2}\right]\right\}.$$

For complete screening, f is given by $f=Z^{1/3}/108$. If one uses f given by

$$f^2=\left(\frac{\epsilon(1+\alpha^2)mc^2}{2E(1-\epsilon)}\right)^2+\left(\frac{Z^{1/3}}{111}\right)^2,$$

then May's formula reduces to the above Schiff formula.

(C) From Olsen and Maximon [Eq. (7.2) in Ref. 7 and formula 2CS in Ref. 6]:

$$d\sigma_{k,\theta}=C\frac{d\epsilon}{\epsilon}\frac{\alpha d\alpha}{(1+\alpha^2)^2}\times\left\{(1-\epsilon)\left[1+\frac{4\alpha^2\Gamma}{(1+\alpha^2)^2}\right]-(1-\epsilon+\tfrac{1}{2}\epsilon^2)(3+2\Gamma)\right\},$$

where

$$\Gamma=\ln(1/\delta)-2-f(Z)+\Im(\delta/\xi),$$

$$\delta=\frac{\epsilon mc^2}{2(1-\epsilon)E},\quad \xi=\frac{1}{1+\alpha^2},$$

$$f(Z)=\left(\frac{Ze^2}{\hbar c}\right)^2\sum_{n=1}^{\infty}\frac{1}{n[n^2+(Ze^2/\hbar c)^2]},$$

[for $Z=13$, $f(Z)=0.0107$; for $Z=79$, $f(Z)=0.3126$], and

$$\Im(\delta/\xi)=\int_{\delta/\xi}^{\infty}\{[1-F(q)]^2-1\}\frac{q^2-(\delta^2/\xi^2)}{q^3}dq,$$

where $F(q)$ is the atom form factor. We have used $\Im(\delta/\xi)$ for the Thomas-Fermi model as used by Molière, which is given by

$$\Im(\delta/\xi)=-\tfrac{1}{2}\sum_{i=1}^{3}\alpha_i^2\ln(1+B_i)+\sum_{\substack{i=1\\ i\neq j}}^{3}\sum_{j=1}^{3}\alpha_i\alpha_j\left[\frac{1+B_j}{B_i-B_j}\ln(1+B_j)+\tfrac{1}{2}\right],$$

with

$$B_i=(\xi Z^{1/3}b_i/121\delta)^2,$$

$$\alpha_1=0.1,\quad \alpha_2=0.55,\quad \alpha_3=0.35,$$

$$b_1=6.0,\quad b_2=1.2,\quad b_3=0.3.$$